



CHORUS

This is the accepted manuscript made available via CHORUS. The article has been published as:

Estimating the Coherence of Noise in Quantum Control of a Solid-State Qubit

Guanru Feng, Joel J. Wallman, Brandon Buonacorsi, Franklin H. Cho, Daniel K. Park, Tao Xin, Dawei Lu, Jonathan Baugh, and Raymond Laflamme

Phys. Rev. Lett. **117**, 260501 — Published 20 December 2016

DOI: [10.1103/PhysRevLett.117.260501](https://doi.org/10.1103/PhysRevLett.117.260501)

Estimating the coherence of noise in quantum control of a solid-state qubit

Guanru Feng,^{1,2} Joel J. Wallman,^{1,3} Brandon Buonacorsi,^{1,2} Franklin H. Cho,^{1,2} Daniel K. Park,^{1,2,4} Tao Xin,^{1,2,5} Dawei Lu,^{1,2} Jonathan Baugh,^{1,2,6,*} and Raymond Laflamme^{1,2,7,8,†}

¹*Institute for Quantum Computing, Waterloo, Ontario, N2L 3G1, Canada*

²*Department of Physics and Astronomy, University of Waterloo, Waterloo, Ontario, N2L 3G1, Canada*

³*Department of Applied Mathematics, University of Waterloo, Waterloo, Canada*

⁴*College of Natural Sciences, Korea Advanced Institute of Science and Technology, Daejeon, 34141, South Korea*

⁵*Department of Physics, Tsinghua University, Beijing 100084, China*

⁶*Department of Chemistry, University of Waterloo, Waterloo, Ontario, N2L 3G1, Canada*

⁷*Perimeter Institute for Theoretical Physics, Waterloo, Ontario, N2J 2W9, Canada*

⁸*Canadian Institute for Advanced Research, Toronto, Ontario M5G 1Z8, Canada*

(Dated: November 21, 2016)

To exploit a given physical system for quantum information processing, it is critical to understand the different types of noise affecting quantum control. Distinguishing coherent and incoherent errors is extremely useful as they can be reduced in different ways. Coherent errors are generally easier to reduce at the hardware level, e.g. by improving calibration, whereas some sources of incoherent errors, e.g. T_2^* processes, can be reduced by engineering robust pulses. In this work, we illustrate how purity benchmarking and randomized benchmarking can be used together to distinguish between coherent and incoherent errors and to quantify the reduction in both of them due to using optimal control pulses and accounting for the transfer function in an electron spin resonance system. We also prove that purity benchmarking provides bounds on the optimal fidelity and diamond norm that can be achieved by correcting the coherent errors through improving calibration.

A key obstacle to realizing scalable quantum information processing (QIP) is implementing quantum gates sufficiently precisely so that errors can be detected and corrected [1–6]. This requires both the intrinsic noise and the noise in the control to be characterized. The combined noise can be completely characterized using either quantum process tomography (QPT) [7, 8] or gate set tomography (GST) [9, 10]. However, these methods are time-consuming and scale exponentially in the number of qubits.

Instead of completely characterizing a system, we can efficiently quantify how noisy the experimental operations are. The most prominent method along these lines is randomized benchmarking (RB) [12–17], which gives an efficient estimate of the benchmarking error per gate (B-EPG) defined as

$$\epsilon(\mathcal{E}) = 1 - F = 1 - \int d\psi \langle \psi | \mathcal{E}(|\psi\rangle\langle\psi|) | \psi \rangle, \quad (1)$$

where \mathcal{E} is the noise channel and the integral (the channel fidelity F) is over all pure states $|\psi\rangle$ according to the Haar measure. However, the B-EPG is, by construction, insensitive to many of the particular details of the noise mechanism. As errors due to different noise mechanisms can be corrected in different ways and have different impacts on QIP, understanding the noise characteristics in quantum systems is of critical importance.

Noise characteristics can be broadly grouped as either coherent (unitary) or incoherent (statistical). Coherent noise is usually due to systematic control errors in, for example, imperfect rotation angles or axes [18, 19], which may be easier to reduce than incoherent noise such as T_1 and T_2 processes. The B-EPG for coherent noise accumulates quadratically with the number of gates whereas incoherent noise accumulates linearly. Furthermore, coherent and incoherent noises with

the same B-EPG may lead to dramatically different thresholds as quantified by the worst-case error per gate (W-EPG), also known as the diamond distance, [20]

$$\epsilon_{\diamond} = \frac{1}{2} \max_{\psi} \|[\mathcal{E} - \mathcal{I}] \otimes \mathcal{I}(\psi)\|_1, \quad (2)$$

where $\|A\|_1 = \text{Tr} \sqrt{A^\dagger A}$ and \mathcal{I} is the identity channel acting on an ancillary system of the same size to account for the effect of the noise on entangled inputs. Therefore, identifying whether the noise is primarily coherent or incoherent is essential for determining an appropriate error threshold when evaluating a physical system and for determining whether experimental effort should prioritize improving calibration or suppressing incoherent error processes.

Several approaches have been developed to provide more information about the noise than just the B-EPG while retaining the advantages of RB [21–24]. In particular, purity benchmarking (PB) [23] enables the quantification of the coherence of a noise process without assuming a specific noise model, which can be used to obtain an improved estimate of the W-EPG [25, 26], whereas the method of Ref. [24] detects additive coherent errors under specific assumptions about the noise model.

In this paper, we show that PB can be used to quantify the best achievable B-EPG and W-EPG under optimal control for single-qubit systems. We then test PB in a specific modality, namely, a solid-state electron spin resonance (ESR) system. Bulk ESR samples consist of an ensemble of (nearly) identical spins, which can mimic the behaviour of a fixed number of qubits depending on the structure of the solid and the species of the spins. ESR provides one path to scalable QIP using techniques such as algorithmic cooling and distributed node quantum information processing [27], which are viable because electron spins have larger thermal polarization

and faster relaxation rates than nuclear spins, and hyperfine-coupled nuclear spins can also be efficiently controlled using ESR techniques [28–30]. The quantum control techniques developed in QIP are also very useful for modern ESR spectroscopy [31, 32]. Achieving high fidelity quantum control in ESR is challenging due to the limited bandwidth of a conventional microwave resonator. In this work, RB and PB protocols are used to assess the control accuracy of an ensemble single-qubit system. We demonstrate the reduction in both the coherent and incoherent errors obtained by first using the transfer function of the microwave control system to correct numerically-derived optimal control (OC) pulses [33] and then using a spin-packet selection technique to effectively reduce the inhomogeneous spectral broadening [34]. The lowest values we obtained for B-EPG (ϵ) and the incoherent error (ϵ_{in} , defined below) for Clifford gates are 6.3×10^{-3} and 5.4×10^{-3} , respectively.

The incoherent error per gate—The primary characteristic of a coherent noise process is that it can be corrected by directly reversing the unitary process with perfect control. We therefore define the incoherent error per gate (I-EPG) of a noise channel \mathcal{E} to be the optimal B-EPG that can be achieved by correcting \mathcal{E} with perfect unitary operations, that is,

$$\epsilon_{\text{in}}(\mathcal{E}) = \min_{\mathcal{U}, \mathcal{V}} \epsilon(\mathcal{U} \circ \mathcal{E} \circ \mathcal{V}) \quad (3)$$

for any unitary operations \mathcal{U} and \mathcal{V} . For a general d -dimensional system, the incoherent error satisfies

$$\epsilon(\mathcal{E}) \geq \epsilon_{\text{in}}(\mathcal{E}) \geq \frac{d-1}{d} \left[1 - \sqrt{u(\mathcal{E})} \right], \quad (4)$$

where the unitarity is [23]

$$u(\mathcal{E}) = \frac{d}{d-1} \int d\psi \text{Tr}[\mathcal{E}(|\psi\rangle\langle\psi| - \frac{1}{d}\mathbb{1}_d)]^2. \quad (5)$$

We now show that the lower bound on the incoherent error in Eq. (4) is saturated to $O[\epsilon_{\text{in}}(\mathcal{E})^2]$ in the single-qubit case. Let $\mathcal{E}_{j,k} = \text{Tr}[\sigma_j^\dagger \mathcal{E}(\sigma_k)]/2$ be the process matrix of \mathcal{E} , where $\{\sigma_0, \sigma_1, \sigma_2, \sigma_3\} = \{\mathbb{1}_2, \sigma_x, \sigma_y, \sigma_z\}$. The process matrix of any completely-positive and trace-preserving (CPTP) noise channel can be written in block form as

$$\mathcal{E} = \begin{pmatrix} 1 & \mathbf{0} \\ \mathcal{E}_n & \mathcal{E}_u \end{pmatrix}. \quad (6)$$

The unitarity and B-EPG of \mathcal{E} are

$$\begin{aligned} u(\mathcal{E}) &= \frac{1}{3} \text{Tr} \mathcal{E}_u^\dagger \mathcal{E}_u \\ \epsilon(\mathcal{E}) &= \frac{1}{6} \text{Tr} (\mathbb{1}_3 - \mathcal{E}_u). \end{aligned} \quad (7)$$

Any single-qubit noise channel can be corrected to another channel \mathcal{E}' such that $\mathcal{E}'_u = \Sigma$ and $\mathcal{E}'_n = (0, 0, \lambda)^T$ for some λ and some real diagonal Σ by applying suitable (perfect) unitary operators [35], which leaves the unitarity unchanged, that

is, $u(\mathcal{E}) = u(\mathcal{E}') = \text{Tr} \Sigma^2$. By Von Neumann's trace inequality,

$$\epsilon(\mathcal{E}') \leq \epsilon(\mathcal{U} \circ \mathcal{E} \circ \mathcal{V}) \quad (8)$$

for any unitary operations \mathcal{U} and \mathcal{V} , so $\epsilon(\mathcal{E}') = \epsilon_{\text{in}}(\mathcal{E})$. Writing $\Sigma = \mathbb{1}_3 - \epsilon(\mathcal{E}')\delta$ where δ is nonnegative for any CPTP map [36] and $\text{Tr} \delta = 6$ from Eq. (7), we have

$$\begin{aligned} u(\mathcal{E}) &= 1 - \frac{2\epsilon(\mathcal{E}')}{3} \text{Tr} \delta + \frac{\epsilon(\mathcal{E}')^2}{3} \text{Tr} \delta^2 \\ &= 1 - 4\epsilon(\mathcal{E}') + (4+c)\epsilon(\mathcal{E}')^2, \end{aligned} \quad (9)$$

for a single qubit. The minimum and maximum values of c subject to $\epsilon(\mathcal{E}') \leq 1/3$, $\text{Tr} \delta = 6$, and the CPTP constraints [17, 36] are 0 and 2, attained when $\delta = 2\mathbb{1}_3$ and $\delta_{1,1} = \delta_{2,2} = 3$ respectively. Therefore the incoherent error for a single qubit satisfies

$$\epsilon_{\text{in}}(\mathcal{E}) = \epsilon(\mathcal{E}') = \frac{1}{2} \left(1 - \sqrt{u(\mathcal{E})} \right), \quad (10)$$

to within $\epsilon_{\text{in}}(\mathcal{E})^2/2$ as claimed.

Now we consider the part of error that is removed by the optimal unitary corrections. With $\mathcal{E} = \mathcal{U} \circ \mathcal{E}' \circ \mathcal{V}$ and $\mathcal{W} = \mathcal{V} \circ \mathcal{U}$, from Eq. (7) the B-EPG of \mathcal{E} is

$$\begin{aligned} \epsilon(\mathcal{E}) &= \frac{1}{6} \text{Tr}(\mathbb{1}_3 - \Sigma) + \frac{1}{6} \text{Tr}(\mathbb{1}_3 - \mathcal{W}_u) \\ &\quad - \frac{1}{6} \text{Tr}(\mathbb{1}_3 - \mathcal{W}_u)(\mathbb{1}_3 - \Sigma) \\ &= \epsilon_{\text{in}}(\mathcal{E}) + \epsilon(\mathcal{W}) + O[\epsilon_{\text{in}}(\mathcal{E})\epsilon(\mathcal{W})] \end{aligned} \quad (11)$$

where the order of the higher-order term comes from Σ being diagonal and the diagonal elements of a generic CPTP map \mathcal{M} being $1 - O(\epsilon(\mathcal{M}))$ [17]. We can regard \mathcal{U} and \mathcal{V} as coherent errors and so the B-EPG of the (composite) coherent error is

$$\epsilon_{\text{coh}}(\mathcal{E}) = \epsilon(\mathcal{W}) = \epsilon(\mathcal{E}) - \epsilon_{\text{in}}(\mathcal{E}) + O(\epsilon_{\text{in}}(\mathcal{E})\epsilon(\mathcal{W})), \quad (12)$$

which is also equivalent [to $O(\epsilon_{\text{in}}(\mathcal{E})\epsilon(\mathcal{W}))$] to the B-EPG removed by the optimal unitary corrections.

The I-EPG also provides an improved bound on the optimal W-EPG $\epsilon_{\diamond, \text{opt}}$ that can be achieved by applying unitary corrections. Let \mathcal{E}'_u be the unital part of \mathcal{E}' , that is, the channel such that $\mathcal{E}'(A) = \mathcal{E}'_u(A) + \lambda\sigma_z \text{Tr} A$ for all $A \in \mathbb{C}^{2 \times 2}$. We then have

$$\mathcal{E}' \otimes \mathcal{I}(\rho) = \mathcal{E}'_u \otimes \mathcal{I}(\rho) + \lambda\sigma_z \otimes \text{Tr}_1 \rho \quad (13)$$

where $\text{Tr}_1 \rho$ is the partial trace over the first system. By the triangle inequality and submultiplicativity of the diamond norm,

$$\begin{aligned} \epsilon_{\diamond}(\mathcal{E}') &\leq \epsilon_{\diamond}(\mathcal{E}'_u) + |\lambda| \max_{\psi} \|\text{Tr}_1 \psi\|_1 \\ &\leq \epsilon_{\diamond}(\mathcal{E}'_u) + \sqrt{2}|\lambda|, \end{aligned} \quad (14)$$

where the maximization is achieved by any maximally entangled state. As \mathcal{E}'_u is a Pauli channel [11, 16], $|\lambda| \leq 3\epsilon(\mathcal{E}')$ and

with a lower bound on the W-EPG in terms of the B-EPG [17], we have

$$\epsilon_{\circ, \text{opt}}(\mathcal{E}) = \epsilon_{\circ}(\mathcal{E}') \in [\frac{3}{2}\epsilon_{\text{in}}(\mathcal{E}), (\frac{3}{2} + 3\sqrt{2})\epsilon_{\text{in}}(\mathcal{E})]. \quad (15)$$

Both these constraints are linear in $\epsilon_{\text{in}}(\mathcal{E})$ and so give reasonable estimates as $\epsilon_{\text{in}}(\mathcal{E})$ decreases compared to the gap between the optimal scalings for the lower and upper bounds in terms of $\epsilon(\mathcal{E})$ alone, which diverge by orders of magnitude as $\epsilon(\mathcal{E})$ decreases [20].

Experimental Implementation—Our X-band pulsed ESR spectrometer was custom-built for QIP experiments and includes arbitrary waveform generation and a loop-gap resonator for sub-millimeter sized samples that allows for relatively broadband control [34]. For an ensemble single-qubit system, we use a sample of gamma-irradiated fused quartz, a paramagnetic sample in powder form where the primary defect is a spin-1/2 unpaired electron at an oxygen vacancy [37], with $T_1 \sim 160 \mu\text{s}$, $T_2 \sim 30 \mu\text{s}$, and $T_2^* \sim 80 \text{ ns}$.

A pulse generated with an initial waveform $W(f)$ in the frequency-domain representation will be distorted to a new waveform $W'(f)$ seen by the spins due to the system's transfer function \mathcal{T} , which is the frequency-domain representation of the impulse response of the system [38, 39], so that $W' = \mathcal{T} \cdot W$ where \cdot denotes the point-wise product of \mathcal{T} and W . The transfer function includes contributions from the resonator's transfer function and other imperfections in the pulse generation and transmission. One method to correct $W'(f)$ is to distort the initial waveform to be $\mathcal{T}^{-1} \cdot W$. The accuracy of this method is limited by the accuracy with which \mathcal{T} can be determined. We measure \mathcal{T} by detecting Rabi oscillations of the electron spins as a function of the microwave frequency [40]. This measured transfer function, denoted by $\mathcal{T}_{\text{meas}}$, is then used to modify the input OC pulse so that the distorted pulse seen by the spins will approximate the desired waveform.

We use three OC pulses: $\pi/2$ and π rotations (denoted by X90, X180, Y90 and Y180 for rotations around the x - and y -axes respectively) and an identity operation (denoted by \mathcal{I}). The pulses are each 150 ns long and designed to be robust to distributions of Larmor frequency and microwave (B_1) field that closely mimic the measured properties of the combined system of our sample and resonator [40]. The design fidelity of each pulse exceeds 99.7% when averaged over these distributions [40]. The experimental results span three different conditions for implementing the OC pulses: (1) not taking the system transfer function into account, *i.e.*, assuming $\mathcal{T} = 1$ for all frequencies, (2) modifying the input pulses using $\mathcal{T}_{\text{meas}}$, and (3) the same as (2) but also implementing a spin-packet selection (SEL) state preparation sequence [34] which effectively increases T_2^* by a factor of 2.

We implement the 24 elements of the Clifford group as $\mathbf{G} = \mathcal{S}\mathcal{P}\mathcal{Z}$ where $\mathcal{S} \in \{\mathcal{I}, \text{X90}, \text{Y90}\}$, $\mathcal{P} \in \{\mathcal{I}, \text{Y180}\}$, and $\mathcal{Z} \in \{\mathcal{I}, \text{Z90}, \text{Z180}, \text{Z270}\}$. \mathcal{S} and \mathcal{P} are implemented using the numerically derived \mathcal{I} , $\pi/2$ and π pulses and altering the phase as needed to achieve x - and y -axis rotations. The operations in \mathcal{Z} are implemented virtually by changing

the reference frame [42]. The initial state in all experiments is represented by the deviation density matrix σ_z .

We can estimate the B-EPG and I-EPG averaged over the set of operations \mathbf{G} via RB and PB as follows [15, 23] (see the quantum circuits in Fig. 1). (1) Prepare the state σ_z . (2) Apply a sequence of m uniformly-random operations from \mathbf{G} , which maps σ_z to ρ_j . (2.1) For RB, apply a recovery gate $R \in \mathbf{G}$ that maps ρ_j back to $\pm\sigma_z$. When the final state is $-\sigma_z$ we change the sign to be positive in post-processing, that is, implement a virtual X gate. (3) For RB, estimate the expectation value $\langle\sigma_z\rangle$. For PB, estimate the purity

$$P = \langle\sigma_x\rangle^2 + \langle\sigma_y\rangle^2 + \langle\sigma_z\rangle^2 \quad (16)$$

of the final state ρ_j . Averaging over random sequences of length m and fitting to

$$\begin{aligned} \langle\sigma_z\rangle &= A_z + B(1 - 2\epsilon)^m \\ \langle P \rangle &= A' + B'u^{m-1} \end{aligned} \quad (17)$$

for RB and PB, respectively, under trace-preserving noise, allows ϵ and the unitarity u (and hence ϵ_{in} via Eq. (10)) to be estimated where the constants absorb the state preparation and measurement (SPAM) errors and the non-unitarity of the noise. In particular, $A' = \sum_M A_M^2$ ($M \in \{\sigma_x, \sigma_y, \sigma_z\}$) with

$$A_M = \text{Tr} M \mathcal{E}(\frac{1}{2}\mathbb{1}_2) = \frac{1}{24} \sum_G \text{Tr} M \mathcal{E}(G\rho G^\dagger), \quad (18)$$

where the summation is over the single-qubit Clifford group and the equality follows from the fact that the Clifford group is a unitary 2-design and hence is also a unitary 1-design [14]. We can therefore estimate both constant off-sets by performing a single Clifford gate, measuring the expectation values of $\langle\sigma_z\rangle$, $\langle\sigma_x\rangle$, and $\langle\sigma_y\rangle$ and averaging over all Clifford gates. The expectation values are measured by the corresponding spin echo detection sequences in Figs. 1(c) and (d). We sample 150 random sequences for each sequence length m of RB and PB independently.

Results and Discussion—The results of the RB and PB experiments are presented in Fig. 2, with the corresponding estimates for the B-EPG, I-EPG, coherent error rate and optimal W-EPG listed in Table I.

Pulse distortion due to the system transfer function is significant, as the transfer function bandwidth of ~ 100 MHz is comparable to the pulse excitation bandwidth. The improvement between results from the unmodified OC pulses ($\mathcal{T} = 1$) and those modified by taking into account $\mathcal{T}_{\text{meas}}$ in Table I demonstrate substantial reduction in ϵ_{coh} from $\sim 10^{-2}$ to $\sim 10^{-3}$. The ϵ_{in} is also reduced by approximately a factor of two, from $\sim 1.0 \times 10^{-2}$ to $\sim 0.5 \times 10^{-2}$. This shows that the pulse distortion is non-negligible, and causes both coherent and incoherent errors. The larger incoherent error for the unmodified OC pulses is largely due to the OC pulses losing their engineered robustness to Larmor frequency and B_1 inhomogeneities when assuming $\mathcal{T} = 1$.

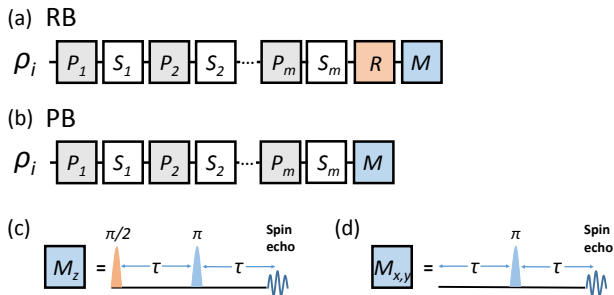


Figure 1. (Color online) Quantum circuits for (a) RB and (b) PB. The initial state ρ_i is σ_z and the measurements M are spin echo detection sequences for measuring $\langle \sigma_z \rangle$ for RB and $\langle \sigma_{x,y,z} \rangle$ for PB. R in (a) is the recovery gate that returns the state to $\pm\sigma_z$. A total of 150 random sequences with $S_j \in \{\mathcal{I}, X90, Y90\}$ and $P_j \in \{\mathcal{I}, X180\}$ (and virtual z -axis rotations) are applied for each sequence length m for RB and PB. (c) and (d) are the spin echo detection sequences for measuring $\langle \sigma_z \rangle$ and $\langle \sigma_{x,y} \rangle$, respectively. The $\pi/2$ and π pulses are 35 ns Gaussian pulses around the y -axis, and $\tau=700$ ns represents a delay.

	$\mathcal{T} = 1$	$\mathcal{T} = \mathcal{T}_{\text{meas}}$	$\mathcal{T} = \mathcal{T}_{\text{meas}}$
	no SEL	no SEL	SEL
ϵ	0.0234(11)	0.0073(2)	0.0063(2)
ϵ_{in}	0.0105(10)	0.0066(2)	0.0054(2)
ϵ_{coh}	0.0119(21)	0.0007(4)	0.0009(4)
$\epsilon_{\diamond, \text{opt}}$	0.040(26)	0.024(15)	0.020(13)

Table I. Estimates of the B-EPG ϵ , I-EPG ϵ_{in} , coherent error rate ϵ_{coh} and optimal W-EPG under perfect calibration $\epsilon_{\diamond, \text{opt}}$ per Clifford gate. Gates are realized with OC pulses that assume a flat resonator transfer function ($\mathcal{T} = 1$) or are distorted based on the measured transfer function ($\mathcal{T} = \mathcal{T}_{\text{meas}}$), and with or without spin packet selection (SEL) sequences respectively. Note that the values listed here are obtained by fitting the RB and PB data to a single-exponential decay, whereas the actual decays are non-exponential, especially noticeable in the $\mathcal{T} = 1$ case. Thus, the estimated gate errors given here are effectively averaged over the non-Markovian noise (see main text).

Although the decay rates of both the RB and PB experimental results are substantially reduced by using $\mathcal{T}_{\text{meas}}$ to improve the OC pulses, the decays seem to deviate from a single exponential decay (i.e., see the oscillating deviations of the orange data points from the orange solid lines in Fig. 2), implying the existence of non-Markovian noise. In our system, the Larmor frequency distribution for different spin-packets (T_2^* effect) results in a significant non-Markovian effect [34, 43]. The benchmarking pulse sequences act like filters, in that the spectral line-width of the part of the spin-packet that contributes to the signal decreases with the number of gates. This means the effective T_2^* lifetime is not constant but increases with the

number of gates that are implemented. Therefore, the error rates estimated using the single-exponential decay model are the averaged values over this non-constant noise. Lindblad numerical simulations (where the T_2^* process is simulated by averaging over multiple simulations with different Larmor frequencies) give non-exponential decays for RB and PB [40], agreeing with our experimental results. To reduce the non-Markovianity due to T_2^* , we implement SEL sequences before each of the benchmarking sequences, which selects a narrower line-width so the benchmarking experiments have a longer T_2^* (~ 160 ns) to begin with [40]. After incorporating the SEL sequences, the experimentally observed decays fit to a single exponential better (see the purple data points and purple dotted lines in Fig. 2). The Lindblad simulation results with the longer T_2^* also exhibit single exponential decays up to ~ 50 gates [40].

Using the SEL sequence improves ϵ_{in} from $(6.6 \pm 0.2) \times 10^{-3}$ to $(5.4 \pm 0.2) \times 10^{-3}$, but has no statistically significant effect on ϵ_{coh} , which is $(0.9 \pm 0.3) \times 10^{-3}$ and $(0.7 \pm 0.4) \times 10^{-3}$ with and without SEL, respectively. This implies the T_2^* effect mainly contributes to the incoherent error. In the Lindblad simulations of the benchmarking sequences using the extended T_2^* , ϵ_{in} caused by T_1 , T_2 , and T_2^* is 3.5×10^{-3} , and ϵ_{coh} caused by the imperfection in the OC pulse design is 0.5×10^{-3} [40]. We attribute the discrepancy between the simulated and experimental values of ϵ_{in} and ϵ_{coh} to possible inaccuracy in the measured decoherence times, fluctuations in the control mechanisms, and imperfect knowledge of the transfer function.

Conclusions– We have demonstrated how RB and PB can be used together to go beyond quantifying average gate fidelities by distinguishing coherent and incoherent contributions to the error. This allows improvements in calibration and engineering pulses to suppress incoherent errors to be implemented and diagnosed independently. Pulse distortion due to the system transfer function \mathcal{T} is the dominant error source in our system and contributes greatly to the coherent part of the gate error. Our measurement of \mathcal{T} helps improve the OC pulse fidelities significantly. The incoherent error is primarily due to T_1 , T_2 and T_2^* processes. By effectively extending T_2^* we reduce the non-Markovian effect and improve the control fidelity further.

Results from gate set tomography included in the supplemental material indicate that our system has substantial gate-dependent noise. The PB protocol has only been analyzed under the assumption of gate-independent noise. Simulations using the estimates from gate set tomography indicate that PB can distinguish between gate-dependent coherent errors that look incoherent when averaged over the gates and a gate-independent incoherent process, at least for some physically-realistic error models. However, we leave the general behavior of PB under gate-dependent noise as an open problem.

Acknowledgement This research was supported by NSERC, the Canada Foundation for Innovation, CIFAR, the province of Ontario, Industry Canada, the Gerald Schwartz & Heather Reisman Foundation, and the U.S. Army Research

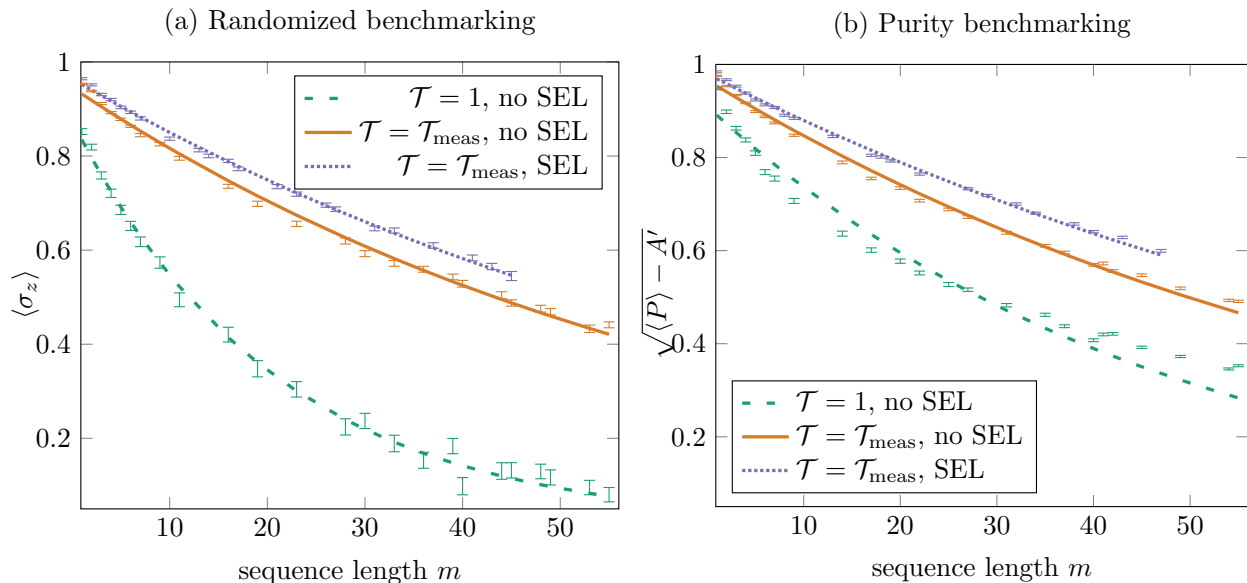


Figure 2. (Color online) Experimental (a) RB and (b) PB results. Each experimental data point of $\langle \sigma_z \rangle$ and $\langle P \rangle$ is an average over 150 random sequences of m Clifford gates where P is defined in Eq. (16), and the error bars indicate the standard error of the mean. The lines are least-squares fits to $\langle \sigma_z \rangle = B(1 - 2\epsilon)^m + A_z$ and $\langle P \rangle = B'u^{m-1} + A' = B'(1 - 2\epsilon_{\text{in}})^{2(m-1)} + A'$, respectively. A_z are 0.0156 ± 0.0005 , 0.0009 ± 0.0010 and -0.0004 ± 0.0013 , and A' are 0.0004 ± 0.0001 , 0.0005 ± 0.0001 and 0.0001 ± 0.0001 , for the three cases ‘ $\mathcal{T} = 1, \text{ no SEL}$ ’ (green dashed line), ‘ $\mathcal{T} = \mathcal{T}_{\text{meas}}, \text{ no SEL}$ ’ (orange solid line), and ‘ $\mathcal{T} = \mathcal{T}_{\text{meas}}, \text{ SEL}$ ’ (purple dotted line), respectively. A_z and A' are estimated using Eq. (18). In (b), $\sqrt{\langle P \rangle - A'}$ is plotted instead of $\langle P \rangle$ to show that $\sqrt{\langle P \rangle - A'}$ has a slower decay than $\langle \sigma_z \rangle$, indicating $\epsilon_{\text{in}} < \epsilon$. The ϵ and ϵ_{in} values are given in Table I. Due to the limitation of the pulsed TWT amplifier, the largest m are 55 and 47 in the cases without and with SEL sequences, respectively. All m are chosen randomly and independently for RB and PB sequences.

Office through grant W911NF-14-1-0103. We thank David Cory and Troy Borneman for providing the ESR sample and for stimulating discussions; Colm Ryan, Yingjie Zhang, and Jeremy Chamilliard for their contributions to the spectrometer; Ming Lyu and Ian Hincks for the discussions on the transfer function measurement method; Robabeh Rahimi for help with preparing the ESR sample; Roberto Romero and Hiruy Haile for help with machining; Hemant Katiyar for help with the simulations.

* baugh@uwaterloo.ca

† laflamme@iqc.ca

- [1] E. Knill, and R. Laflamme, Phys. Rev. A 55 (2), 900 (1997).
- [2] E. Knill, R. Laflamme, and W. H. Zurek, Science 279 (5349), 342–345 (1998).
- [3] J. Preskill, Proceedings of the Royal Society of London. Series A: Mathematical, Physical and Engineering Sciences 454 (1969), 385–410 (1998).
- [4] E. Knill, Nature 434 (7029), 39–44 (2005).
- [5] P. Aliferis, D. Gottesman, and J. Preskill, Quantum Information & Computation 8 (3), 181–244 (2008).
- [6] D. Gottesman, Stabilizer codes and quantum error correction. caltech ph. d, Ph.D. thesis, Thesis, eprint: quant-ph/9705052 (1997).
- [7] I. L. Chuang, and M. A. Nielsen, J. Mod. Opt. 44, 2455 (1997).
- [8] J. F. Poyatos, J. I. Cirac, and P. Zoller, Phys. Rev. Lett. 78, 390 (1997).
- [9] S. T. Merkel, J. M. Gambetta, J. A. Smolin, S. Poletto, A. D. Córcoles, B. R. Johnson, C. A. Ryan, and M. Steffen, Phys. Rev. A 87, 062119 (2013).
- [10] R. Blume-Kohout, J. K. Gamble, E. Nielsen, J. Mizrahi, J. D. Sterk, and P. Maunz, arXiv:1310.4492 (2013).
- [11] S. Kimmel, M. P. da Silva, C. A. Ryan, B. R. Johnson, and T. Ohki, Phys. Rev. X 4, 011050 (2014).
- [12] J. Emerson, R. Alicki, and K. Życzkowski, Journal of Optics B: Quantum and Semiclassical Optics 7 (10), S347 (2005).
- [13] E. Knill, D. Leibfried, R. Reichle, J. Britton, R. B. Blakestad, J. D. Jost, C. Langer, R. Ozeri, S. Seidelin, and D. J. Wineland, Phys. Rev. A 77, 012307 (2008).
- [14] C. Dankert, R. Cleve, J. Emerson, and E. Livine, Phys. Rev. A 80 (1), 012304 (2009).
- [15] E. Magesan, J. M. Gambetta, and J. Emerson, Phys. Rev. Lett. 106, 180504 (2011).
- [16] E. Magesan, J. M. Gambetta, and J. Emerson, Phys. Rev. A 85, 042311 (2012).
- [17] J. J. Wallman, and S. T. Flammia, New J. Phys. 16, 103032 (2014).
- [18] J. J. L. Morton, A. M. Tyryshkin, A. Ardavan, K. Porfyarakis, S. A. Lyon, and G. A. D. Briggs, Phys. Rev. A 71, 012332 (2005).
- [19] S. Kimmel, G. H. Low, and T. J. Yoder, Phys. Rev. A 92, 062315 (2015).
- [20] Y. R. Sanders, J. J. Wallman, and B. C. Sanders, New J. Phys. 18, 012002 (2015).
- [21] J. J. Wallman, M. Barnhill, and J. Emerson, Phys. Rev. Lett. 115, 060501 (2015).
- [22] P. J. J. O’Malley *et al.*, Phys. Rev. Appl. 3, 044009 (2015).
- [23] J. J. Wallman, C. Granade, R. Harper, and S. T. Flammia, New J. Phys. 17, 113020 (2015).

- [24] S. Sheldon *et al.*, Phys. Rev. A 93, 012301 (2016).
- [25] J. J. Wallman, arXiv:1511.00727 (2015).
- [26] R. Kueng, D. M. Long, A. C. Doherty, and S. T. Flammia, arXiv:1510.05653 (2015).
- [27] T.W. Borneman, C.E. Granade, D.G. Cory, Phys. Rev. Lett. 108 (14), 140502 (2012).
- [28] J. S. Hodges, J. C. Yang, C. Ramanathan, and D. G. Cory, Phys. Rev. A 78 (1), 010303 (2008).
- [29] Y. Zhang, C. A. Ryan, R. Laflamme, and J. Baugh, Phys. Rev. Lett. 107 (17), 170503 (2011).
- [30] D. K. Park, G. Feng, R. Rahimi, S. Labrüyère, T. Shibata, S. Nakazawa, K. Sato, T. Takui, R. Laflamme, and J. Baugh, Quantum Information Processing 14 (7), 2435–2461 (2015).
- [31] T. Prisner, M. Rohrer, and F. MacMillan, Annu. Rev. Phys. Chem. 52, 279 (2001).
- [32] P.E. Spindler, Y. Zhang, B. Endeward, *et al.*, J. Magn. Reson. 218, 4958 (2012).
- [33] N. Khaneja, T. Reiss, C. Kehlet, T. Schulte-Herbrüggen, and S. J. Glaser, Journal of Magnetic Resonance 172 (2), 296–305 (2005).
- [34] D. K. Park, G. Feng, R. Rahimi, J. Baugh, and R. Laflamme, Journal of Magnetic Resonance 267, 68–78 (2016).
- [35] C. King, and M. B. Ruskai, J. Math. Phys. 42, 87–98 (2001).
- [36] M. B. Ruskai, S. Szarek, and E. Werner, Linear Algebr. Appl. 347 159 (2002).
- [37] S. Eaton, and G. Eaton, Journal of Magnetic Resonance, Series A 102 354 – 356 (1993).
- [38] T. Kaufmann *et al.*, J. Magn. Reson. 235, 95–108 (2013).
- [39] S. Gustavsson, O. Zwier, J. Bylander, F. Yan, F. Yoshihara, Y. Nakamura, T. P. Orlando, and W. D. Oliver, Phys. Rev. Lett. 110, 040502 (2013).
- [40] See Supplemental Material [url], which includes Ref. [41].
- [41] [reference in Supplemental Material not already in Letter] J. M. Chow *et al.*, Phys. Rev. Lett. 109, 060501 (2012).
- [42] C. A. Ryan, M. Laforest, and R. Laflamme, New J. of Phys. 11 (1), 013034 (2009).
- [43] M. A. Fogarty, M. Veldhorst, R. Harper, C. H. Yang, S. D. Bartlett, S. T. Flammia, and A. S. Dzurak, Phys. Rev. A 92, 022326 (2015).